Scale effect in mechanical characterization of WC-Co composites

D.A. Sandoval, A. Rinaldi, J.M. Tarragó, J.J. Roa, J. Fair, L. Llanes

PII: S0263-4368(17)30772-2
DOI: https://doi.org/10.1016/j.ijrmhm.2017.12.029
Reference: RMHM 4627

To appear in: *International Journal of Refractory Metals and Hard Materials*

Received date: 18 October 2017
Revised date: 15 December 2017
Accepted date: 18 December 2017

Please cite this article as: D.A. Sandoval, A. Rinaldi, J.M. Tarragó, J.J. Roa, J. Fair, L. Llanes , Scale effect in mechanical characterization of WC-Co composites. The address for the corresponding author was captured as affiliation for all authors. Please check if appropriate. Rmhm(2017), https://doi.org/10.1016/j.ijrmhm.2017.12.029

Scale effect in mechanical characterization of WC-Co composites

D.A. Sandoval [a,b,*], A. Rinaldi [c], J.M. Tarragó [d,1], J. J. Roa [a,b], J. Fair [e], L. Llanes [a,b]

[a] CIEFMA-Department of Materials Science and Metallurgy, EEBE-Campus Diagonal Besòs, Universitat Politècnica de Catalunya, Barcelona (Spain).

[b] Barcelona Research Center in Multiscale Science and Engineering, Campus Diagonal Besòs, Universitat Politècnica de Catalunya, Barcelona (Spain)

[c] Italian National Agency for New Technologies, Energy and Sustainable Economic Development (ENEA), Casaccia. Rome (Italy)

[d] Rock Tools R&D, Sandvik Mining and Rock Technology, Stockholm (Sweden)

[e] Sandvik Hyperion, Coventry (United Kingdom)

*Corresponding author

Address: CIEFMA-Department of Materials Science and Metallurgy, EEBE-Campus Diagonal Besòs, Universitat Politècnica de Catalunya, 08930, Barcelona (Spain)

E-mail: daniela.andreina.sandoval@upc.edu

[1] Current address: Sandvik Hyperion, 08107, Barcelona (Spain)

Abstract

The study of mechanical response of materials at small length scales has gained importance due to the recent advances in micro- and nano-fabrication as well as testing systems. However, most of the reported work has been dedicated to investigate single-crystals or boundary-containing metallic systems, while much less attention has been paid to composite materials, and in particular those combining soft and hard phases. In this work, a systematic procedure is followed for machining micropillars of diameters ranging from 1 to 4 μm in a WC-Co composite with a WC mean grain size around 1 μm, by means of focused ion beam milling. In-situ uniaxial compression of the micropillars and subsequent field emission scanning electron microscopy inspection were conducted. Clear size effects are evidenced. Smaller test specimens (probe size approaching the mean WC size) exhibit deformation/failure mechanisms observed for WC crystals; while for bigger sample sizes, the mechanical response involves several mechanisms directly linked with the microstructural characteristics of the bulk-like cemented carbide material. On the other hand, independent of micropillar size, carbide-carbide or carbide-binder interfaces are found to be preferential sites for nucleation of critical damage events.

Keywords

WC-Co, size effect, micropillar, uniaxial compression, plastic deformation, failure mechanisms.

1. Introduction

Intrinsic properties of crystalline materials such as yield stress, can be greatly influenced by extrinsic factors such as volume. For instance, results have evidenced an inverse relation between the hardness and the indentation depth at the micro- and nanometric length scales, as has been previously summarized elsewhere [1,2]. Yield stress of single crystals with different pillar diameters tends to increase when decreasing the sample size, thus exhibiting a behavior quite different from that expected for macroscopic behavior [1–3]. For other testing configurations, similar trends have been found. For torsion it was shown that the steeper the strain gradient, the greater the hardening; therefore, hardness measured at the micrometric length scale showed higher values than that at millimeter scale [4]. Moreover, a strong size effect has been found in bending [5] and tension [6] tests of micron-sized beams.

During the last decade, special attention has being paid to the micropillar compression approach because of its advantages. First, the stress-state is nominally uniaxial, allowing a straight conversion of the measured load (*P*)-displacement (*h*) data into flow curves [7]. Second, sample preparation by means of Focused Ion Beam (FIB) milling [8] may be described as a relatively easy machining route. Finally, it involves the use of a conventional nanoindenter with a flat-end tip either ex-situ or in-situ by using Scanning Electron Microscopy (SEM) or Transmission Electron Microscopy (TEM) techniques [9]. On the other hand, some limitations can be mentioned such as micropillar taper angle, possible misalignment of the flat punch, and the presence of friction forces that can contribute to a non-uniform stress state [7,10]. Within this context, micropillar compression has been widely used to study the mechanical response of metallic single crystals [1,11], metallic alloys [12] and metallic nanolaminates [3,13], among others. However, similar studies involving composite materials, and particularly those including soft and hard phases, are quite scarce. Key materials within this group are WC-Co cemented carbides (usually referred to as hardmetals), the most successful

example of the optimal implementation of microstructural design, on the basis of composite synergy, towards enhanced performance and reliability in extremely demanding applications (e.g. Refs. [14–16]). Regarding these materials, three recent investigations addressing micromechanical testing may be highlighted. Csanádi *et al.* [17] reported the deformation characteristics of WC by performing micropillar compression on particles oriented parallel and perpendicular to the basal plane. Trueba *et al.* [18] showed the different cracking events that occur in a WC-Co grade when bending microbeams. Finally, Tarragó *et al.* [19] evidenced prominent glide and fracture events within the binder adjacent to interfaces with WC particles and in the WC/metallic binder interfaces. In all these studies, the effect of the probe size and its possible relation with the microstructure has not been addressed. Moreover, testing protocols has not been defined for detailed study of the mechanical behavior of cemented carbides at such small length scales. The aim of this study is to bring insights on the scale effect on the mechanical response of WC-Co composites and develop the protocols for detailed study of the micromechanical behavior of heterogeneous materials, such as cemented carbides. In doing so, tests are proposed aiming to correlate probe size, in terms of the amount of WC confined within the effective section of the micropillars, with the mechanisms of deformation and failure observed after uniaxial compression.

2. Materials and methods

The material studied is a commercial grade of WC-Co supplied by Sandvik Hyperion, with 11 *wt.%* of Co (17 vol.%) and the following microstructural characteristics: mean carbide grain size (d_{WC}) of 1.1 ± 0.7 μm; binder mean free path (λ_{Co}) of 0.4 ± 0.3 μm and WC contiguity (C_{WC}) of 0.4 ± 0.1. The magnetic cobalt of the material was assessed, and a 9.9% value was obtained. This value indicates that the material is within the two phase carbon window but in a region relatively close to the eta-phase border (i.e. low C content). Mean carbide grain size was measured by linear intercept method using field emission scanning electron microscopy (FESEM) micrographs obtained with a JEOL-7001F unit. Carbide contiguity and binder mean free path were obtained by following the expressions proposed by Torres [20], Coureaux [21] and Tarragó *et al.* [22] in which basic empirical relationships proposed by Roebuck and Almond [15] where modified to include carbide size influence. Before the milling, the sample surface was ground and diamond polished up to mirror-like surface finish following a 6 μm to 1 μm sequence, with a final stage of polishing with colloidal silica.

The milling process was done in several stages, depending on the aimed diameter of the micropillar, with a dual beam Zeiss Neon 40 Focused Ion Beam - Field Emission Electron Microscope (FIB/FESEM) with a Ga^+ ion source operated at 30 kV. A total of three micropillars of around 1, 2 and 4 μm in diameter were milled. Aspect ratio of the micropillars (l_{pillar}/d_{pillar}) was held constant and around 2.5, and taper angles were kept less than 5°. The resulting micropillars were uniaxially compressed in-situ using a nanoindenter INSEM Nanomechanics Inc., placed inside a high-resolution Field-Emission-Gun SEM (FEG-SEM, LEO 35, Zeiss) and equipped with a flat-diamond punch of 5 μm in nominal diameter. The tests were done under displacement control mode. *P-h* data was continuously recorded during the tests. Nominal stresses (σ) and strains (ε) were directly calculated from the *P-h* data. The diameter of the pillar at 1 μm of depth from the surface was chosen to calculate stresses, in order to avoid possible milling effects, and because the maximum deformation occurs in this region. For an accurate estimation of the strains, the effective elastic

deformation of both the indenter and the bulk material below the micropillar should be extracted using an approach derived by Sneddon [17,18], according to the following expression:

$$x_{Sneddon} = (1-v_i^2/E_i)*(F_{meas}/d_t) + (1-v_b^2/E_b)*(F_{meas}/d_b) \quad (1)$$

where $x_{Sneddon}$ is the displacement corrected by the Sneddon's approach, F_{meas} is the measured force, d_t and d_b are the diameters of the micropillar at the top and bottom respectively; Young's modulus and Poisson's ratio of the diamond tip are E_i and v_i, and taken to be 1140 GPa and 0.07 respectively [25]; and Young's modulus and Poisson's ratio of the bulk are E_b and v_b, and taken to be 577 GPa and 0.24 respectively [26]. Calibration of the machine compliance was done on fused silica of known elastic modulus (72 GPa) [25], using a Berkovich tip. By uniaxial compression of micropillars of fused silica, of known geometry, the estimated machine compliance (displacement from the compliance of the equipment) was verified to be the same for the flat punch. An additional correction for the equipment compliance was taken into account by assuming that the measured displacement followed the expression:

$$x_{meas} = x_{Sneddon} + x_{pillar} + x_{equip} \quad (2)$$

where x_{meas} is the measured displacement, x_{pillar} is the displacement of the pillar of fused silica, and x_{equip} is displacement from the compliance of the equipment.

After the in-situ uniaxial compression, the micropillars were observed and sectioned by means of FESEM and FIB respectively, in order to detect deformation and failure mechanisms induced by the tests, at the

surface and inside the micropillars. Images taken during sectioning were used to estimate the volume percent of WC phase within the micropillars, by means of image analysis (IA) and using the free software FIJI ImageJ2.

3. Results and discussion

3.1 *Design of micro-compression experiments in cemented carbides*

Micropillar compression is a relatively new experimental technique used mostly in metallic single crystal materials. Within this context, studies have discussed the accurate way to design such experiments due to experimental constraints [7,10]. To the best knowledge of the authors, such studies are rather scarce for polycrystalline materials, and even more limited for composites. In this regard, the mechanical behavior should be expected to be influenced by the size of the sample. For example, for single-crystal micropillars of metals, an inverse power-law has been found between the critical resolved shear stress along the slip plane and the pillar diameter [21,22]. For polycrystalline materials a combination of intrinsic and extrinsic length scales affects the overall behavior. In metallic materials, two responses can be observed depending on the sample size, grain size and dislocation density [29]. On one hand, a strain-hardening response that follows a Hall-Petch correlation; and on the other hand, source-limited plasticity, leading to a “smaller is stronger” behavior. Regarding cemented carbides, a Hall-Petch relationship has been found for the constrained binder, implying that as the mean free path gets smaller, the effective flow stress on the binder is higher, given that the carbides act as strong grain boundaries impeding dislocation motion [30].

3.1.1 *Surface finish*

Given the difference in hardness of the constitutive phases of cemented carbides, mechanical polishing can result in surface roughness ranging between 300 and 500 nm, measured by Atomic Force Microscopy (AFM), where carbide particles are in a higher level than the Co binder, depending on the method and microstructural characteristics of the hardmetal grade. For small scale micro-compression, high roughness can lead to non-uniform contact of the flat-punch with the surface of the micropillar, causing a non-uniaxial compression. Thus, outer WC particles can induce deformation in the inner Co binder. To reduce this effect,

the two final steps of the polishing process were consecutively done for multiple times (up to 8) until a surface roughness of less than 10 nm was obtained.

3.1.2 *Micropillar milling*

The main micropillar parameter to take into consideration during the micropillar milling is the aspect ratio, defined as the ratio between the pillar length and its surface diameter. This parameter can magnify the pillar sink-in upon compression, which leads to an inaccurate measurement of the pillar deformation. Moreover, high aspect ratio can lead to premature buckling of the pillar. In this regard, it has been shown that aspect ratios higher than 2 [10] and taper angle less than 5° [31] have negligible effect in the calculated stress ans strain data. In order to achieve an aspect ratio ranging between 2 and 4, and taper angles smaller than 5°, the milling has to be done in a two-step process for micropillars of 1 and 2 µm in diameter, with currents of 10 nA for the broad milling, and 500 pA for the fine milling. For the micropillars of 4 µm an additional intermediate milling step, with current of 2 nA had to be done in order to reduce the exposure time and reduce the amount of Ga^+ implanted on the micropillars surface. Final aspect ratios and taper angles obtained for each micropillar diameter are summarized in **Table I**.

FESEM images fo one final milled micropillar for each diameter can be seen in **Fig. 1**. The lighter phase corresponds to WC phase, while the darker gray (evidenced in **Fig. 1 b and c**), corresponds to the Co binder phase. As it can be depicted in this image, when the size of the micropillar in terms of diameter and length increases, the micropillar base is more sunk into the bulk. It hinders the accurate measure of the micropillar length because the effective level of the referred base may not be defined precisely. This phenomenon may be associated with the annular milling methodology employed for this study. For this particular case, it can be related to the dwell time for each sample, defined as the time of incidence of the beam per pixel, i.e. the depth milled per pixel [32]. In this study, the pixel size was kept constant for the fine

milling of the micropillars and equals to 25 nm per pixel. Therefore, for a given current, dwell time was varied being longer for the larger micropillars, to obtain the desired length.

Moreover, the phase distribution in each size micropillars is expected to play a significant role in its mechanical response when being uniaxially compressed. Accordingly, it is expected that as the micropillars diameter approaches the carbide mean grain size (d_{WC}), less binder can be found within the specimens. Thus, as the diameter of the micropillars increases, its phase distribution approaches that of the bulk. However, being a microstructurally heterogeneous material, the phase distribution may vary depending on the region chosen for milling the micropillars. In this regard, it was considered that the 1 μm micropillar contained 100 vol.% of WC given that the micropillar diameter approached d_{WC} and evidence of binder phase was scarcely found in its surface.

3.2 *Uniaxial compression of micropillars*

In order to induce surface detectable damage in the micropillars, several tests were done by varying the maximum imposed strains and the maximum indentation load. Catastrophic failure was observed for the 1 μm in diameter specimens. Peak levels reached during testing for each diameter condition are summarized in **Table II**.

Deformation mechanisms observed in micropillars with a diameter comparable with the WC mean grain size can be expected to be those observed on a single WC grain, with a given crystallographic orientation perpendicular to the compression axis. On the other hand, for larger diameter micropillars, final failure should be expected to result from a combination of events, closer to the scenario usually seen in the bulk material.

FESEM micrographs for one of the micropillars of 1, 2 and 4 μm in diameter, after uniaxial compression, are shown in **Fig. 2 a, b and c** respectively. White arrows show the most noticeable deformation/failure mechanisms. Even though the 1 μm pillar failed catastrophically, slip lines are visible at the bottom of the pillar and near 45° with respect to the compression axis (**Fig. 2 a**). This type of slip system has been found for WC micropillars with axes perpendicular to the prismatic plane, also leading to the failure of the pillar [17]. Furthermore, slip bands at around 50° can also be evidenced for one carbide, near the top of the micropillars with 2 and 4 μm in diameter (**Fig. 2 b and c**). Such slip systems have been associated with a splitting dislocation reaction of 1/3<$1\bar{2}13$> dislocations into 1/6<$1\bar{2}13$> partial dislocations in the {$10\bar{1}0$} prismatic plane [33]. An additional Transmission Electron Microscopy (TEM) study should be done to identify the specific deformation mechanisms.

Deformation/failure scenario observed for the 2 μm and 4 μm in diameter micropillar are depicted in **Fig. 2b and 2c**, respectively. Among them, plastic flow of the Co binder, glide between WC/WC particles and related emergence of cracks appear to be the major deformation/fracture mechanisms. These observations would support the idea that WC/WC interfaces are weak points for failure in cemented carbides [34]. Plastic flow of the Co binder, clearly seen for the 2 μm micropillar, and evidenced as the lighter phase that frames some WC particles for the 4 μm micropillar, can be a consequence of less effective constraint of the Co binder by WC particles. In this regard, for small volume of samples, the microstructural characteristics defined for the bulk material, such as the binder mean free path can differ, therefore, the micropillar volume cannot be representative of the bulk scenario. In this study it was found that volume fractions of WC in 2 μm (85 ± 5 vol.%) and 4 μm (81 ± 7 vol.%) micropillars, do not differ considerably from that of the bulk material (83 vol.%). Thus, constraint degree of the Co binder can differ from one micropillar to another, depending on the ratio d_{pillar}/d_{WC} and on location of binder pools, i.e. binder pools located inside the micropillar are more constrained by the surrounding WC particles.

From the images taken by FIB sectioning (**Fig. 3 a and b**), it is observed that small cracks (on the order of hundreds of nanometers) probably emerged in and extended along WC/WC interfaces, as well as into the metallic binder, where they continued to propagate. These observations are in agreement with previous findings by Tarragó *et al.* [19], who pointed out that cracks were found to run very close to WC/Co interfaces, but within the binder and parallel to the phase boundary due to the coincidence of high plastic strains and maximum triaxiality conditions [35].

Furthermore, bands in a different grey scale can be appreciated within the Co binder phase. In order to understand better the nature of such bands, a trench was milled by FIB on the bulk material. FESEM/FIB images were taken in the same conditions as for the micropillars: 30 kV accelerating voltage and tilted 36 degrees (**Fig. 4**). The bands are present in both FESEM and FIB images, suggesting that under these conditions, channeling contrast is achieved; and therefore, substructural features associated with crystallographic differences can be discerned [36]. The presence of the different gray scale bands in the Co binder in the bulk material suggests that there exists Co with both fcc and hcp crystal configurations in the material before micropillar milling and uniaxial compression. Furthermore, deformation within the Co binder can occur through other mechanisms as planar slip, twinning or from deformation-induced phase transformation (from fcc to hcp structure), as they have been observed in previous works reported in the literature [37–41]. However, the extent of the deformation of the Co binder after uniaxial compression, must be evaluated by means of TEM, and it will be addressed in future research.

σ-ε curves representative of the micropillars tested for the three diameters are shown in **Fig. 5**. Elastic modulus (E) of the bulk, measured from its stiffness (around 210 and 700 GPa for the Co binder and the WC, respectively) [42], are shown for comparison purposes. From the unloading curves it can be seen than for both 2 μm and 4 μm in diameter specimens, the elastic modulus is confined between the values for

individual phases. From the 1 μm micropillar curve it is evidenced that yielding events (pop-ins) occur at much higher stresses than for the 2 and 4 μm micropillars. Such yielding events, between 6.5 and 7 GPa, can be associated with the plastic deformation observed in **Fig. 2 a**. Moreover, rupture stress (σ_r) reached values of around 7.2 GPa, in good agreement with those found by Csanádi *et al.* [17] for WC single crystals oriented in the prismatic plane perpendicular with respect to the applied load. From the load curves for the 2 μm micropillar, yielding events can be depicted between 2.7 and 4 GPa. Such values are within the range of flow stresses values reported for highly constrained Co binder (between 2.2 and 3.7 GPa) [34,35]. Findings by Tarragó *et al.* [19] showed that for a WC-Co grade with λ_{Co} around 0.8 μm, plastic flow of the Co binder occurred at smaller stresses. For the 4 μm micropillar, a less evident yielding event took place at around 2.3 GPa. It could be also related to the plastic flow of less constraint binder. Following the above ideas, it may be stated that the mechanical response of WC-Co cemented carbides at small scales is highly influenced by the degree of constraint of the Co binder. However, it should be mentioned that phenomena developed when compressing WC-Co micropillars may also involve the influence of other microstructural parameters such as volume fraction of each phase and crystallographic orientation of the WC particles contained in the micropillar, as well as fcc/hcp ratio of Co binder before uniaxial compression.

Data obtained showed the great influence of the microstructural aspects on the mechanical response of cemented carbides at small length scales. Furthermore, it is evidenced the scale effect: smaller test specimens exhibited deformation/failure mechanisms observed for plain WC crystals, while for bigger sample sizes, the mechanical response involve several mechanisms directly linked with the microstructural characteristics of the bulk-like material. Moreover, a sample size with a greater contact area (nearly four times d_{WC}), showed a behavior that resembles that of the bulk material when been compressed. In general, micromechanical testing of cemented carbides brings insights of the phenomena developed locally, and especially at the WC/WC and WC/Co interfaces.

4. Summary and concluding remarks

WC-Co micropillars of different size in diameter were milled by means of FIB. In doing so, a systematic milling protocol was developed in order to achieve a standardized process to mill micropillars for uniaxial compression of cemented carbides. As expected, as the probe size increases, the phase distribution approaches that of the bulk. Thus, it was observed that deformation/failure mechanisms for a probe size approaching the WC mean grain size are consistent with those observed for a single WC grain. On the other hand, for a sample size twice and four times bigger, the mechanical response under uniaxial compression exhibits a combination of several deformation and failure mechanisms which can approach the behavior of the bulk. It supports the existence of scale effects, within the context of the testing protocol here implemented. The observed mechanisms lead to infer that the degree of constraint of the Co binder strongly affect early yielding. Furthermore, it is clearly discerned that WC/WC and WC/Co interfaces are preferential sites for irreversible deformation and failure phenomena.

5. Acknowledgements

This work was partially funded by the Spanish Ministerio de Economía y Competitividad (MINECO/FEDER) through Grant MAT2015-70780-C4-3-P, and by the industry-university collaborative program between Sandvik Hyperion and UPC. D.A. Sandoval would like to acknowledge the support received by the COST Action CA15102 “Solutions for Critical Raw Materials under Extreme Conditions” as funding for a Short Term Scientific Mission at ENEA, and Trifon Trifinov at Barcelona research Center in Multiscale Science and Engineering, for the support with FIB milling and sectioning of the micropillars.

6. References

[1] M.D. Uchic, Sample dimensions influence strength and crystal plasticity, Science (80-.). 305 (2004) 986–989. doi:10.1126/science.1098993.

[2] J.L. Stewart, L. Jiang, J.J. Williams, N. Chawla, Prediction of bulk tensile behavior of dual phase stainless steels using constituent behavior from micropillar compression experiments, Mater. Sci. Eng. A. 534 (2012) 220–227. doi:10.1016/j.msea.2011.11.062.

[3] D.R.P. Singh, N. Chawla, G. Tang, Y.L. Shen, Micropillar compression of Al/SiC nanolaminates, Acta Mater. 58 (2010) 6628–6636. doi:10.1016/j.actamat.2010.08.025.

[4] N.A. Fleck, G.M. Muller, M.F. Ashby, J.W. Hutchinson, Strain gradient plasticity: Theory and experiment, Acta Metall. Mater. 42 (1994) 475–487. doi:10.1016/0956-7151(94)90502-9.

[5] C. Motz, T. Schöberl, R. Pippan, Mechanical properties of micro-sized copper bending beams machined by the focused ion beam technique, Acta Mater. 53 (2005) 4269–4279. doi:10.1016/j.actamat.2005.05.036.

[6] M.D. Uchic, D.M. Dimiduk, J.N. Florando, W.D. Nix, Exploring specimen size effects in plastic deformation of Ni3(Al, Ta), MRS Proc. 753 (2002) 1–6. doi:10.1557/PROC-753-BB1.4.

[7] D. Kiener, C. Motz, G. Dehm, Micro-compression testing: A critical discussion of experimental constraints, Mater. Sci. Eng. A. 505 (2009) 79–87. doi:10.1016/j.msea.2009.01.005.

[8] M.D. Uchic, D.M. Dimiduk, A methodology to investigate size scale effects in crystalline plasticity using uniaxial compression testing, Mater. Sci. Eng. A. 400–401 (2005) 268–278. doi:10.1016/j.msea.2005.03.082.

[9] M. Legros, D.S. Gianola, C. Motz, Quantitative in situ mechanical testing in electron microscopes,

MRS Bull. 35 (2010) 354–360. doi:10.1557/mrs2010.567.

[10] H. Zhang, B.E. Schuster, Q. Wei, K.T. Ramesh, The design of accurate micro-compression experiments, Scr. Mater. 54 (2006) 181–186. doi:10.1016/j.scriptamat.2005.06.043.

[11] H. Tang, K. Schwarz, H. Espinosa, Dislocation escape-related size effects in single-crystal micropillars under uniaxial compression, Acta Mater. 55 (2007) 1607–1616. doi:10.1016/j.actamat.2006.10.021.

[12] H. Bei, S. Shim, E.P. George, M.K. Miller, E.G. Herbert, G.M. Pharr, Compressive strengths of molybdenum alloy micro-pillars prepared using a new technique, Scr. Mater. 57 (2007) 397–400. doi:10.1016/j.scriptamat.2007.05.010.

[13] N.A. Mara, D. Bhattacharyya, P. Dickerson, R.G. Hoagland, A. Misra, Deformability of ultrahigh strength 5nm Cu/Nb nanolayered composites, Appl. Phys. Lett. 92 (2008) 231901. doi:10.1063/1.2938921.

[14] H.E. Exner, Physical and chemical nature of cemented carbides, Int. Mater. Rev. 4 (1979) 1149–73.

[15] B. Roebuck, E.A. Almond, Deformation and fracture processes and the physical metallurgy of WC-Co hardmetals, Int. Mater. Rev. 33 (1988) 90–112.

[16] L. Prakash, Fundamentals and General Applications of Hardmetals, in: V.K. Sarin, D. Mari, L. Llanes (Eds.), Compr. Hard Mater. Vol. 1, Elsevier Ltd, UK, 2014: pp. 29–90.

[17] T. Csanádi, M. Bľanda, A. Duszová, N.Q. Chinh, P. Szommer, J. Dusza, Deformation characteristics of WC micropillars, J. Eur. Ceram. Soc. 34 (2014) 4099–4103. doi:10.1016/j.jeurceramsoc.2014.05.045.

[18] M. Trueba, A. Aramburu, N. Rodríguez, I. Iparraguirre, M.R. Elizalde, I. Ocaña, J.M. Sánchez, J.M. Martínez-Esnaola, “In-situ” mechanical characterisation of WC-Co hardmetals using microbeam

testing, Int. J. Refract. Met. Hard Mater. 43 (2014) 236–240. doi:10.1016/j.ijrmhm.2013.12.005.

[19] J.M. Tarragó, J.J. Roa, E. Jiménez-Piqué, E. Keown, J. Fair, L. Llanes, Mechanical deformation of WC–Co composite micropillars under uniaxial compression, Int. J. Refract. Met. Hard Mater. 54 (2016) 70–74. doi:10.1016/j.ijrmhm.2015.07.015.

[20] Y. Torres, Comportamiento a fractura y fatiga de carburos cementados WC-Co, Barcelona, 2002.

[21] D. Coureaux, Comportamiento mecánico de carburos cementados WC-Co: Influencia de la microestructura en la resistencia a la fractura, la sensibilidad a la fatiga y la tolerancia al daño inducido bajo solicitaciones de contacto., Universitat Politècnica de Catalunya, 2012.

[22] J.M. Tarragó, D. Coureaux, Y. Torres, F. Wu, I. Al-Dawery, L. Llanes, Implementation of an effective time-saving two-stage methodology for microstructural characterization of cemented carbides, Int. J. Refract. Met. Hard Mater. 55 (2016) 80–86. doi:10.1016/j.ijrmhm.2015.10.006.

[23] B. Poon, D. Rittel, G. Ravichandran, An analysis of nanoindentation in linearly elastic solids, Int. J. Solids Struct. 45 (2008) 6018–6033. doi:10.1016/j.ijsolstr.2008.07.021.

[24] C.A. Volkert, E.T. Lilleodden, Size effects in the deformation of sub-micron Au columns, Philos. Mag. 86 (2006) 5567–5579. doi:10.1080/14786430600567739.

[25] W.C. Oliver, G.M. Pharr, An improved technique for determining hardness and elastic modulus using load and displacement sensing indentation experiments, J. Mater. Res. 7 (1992) 1564–1583.

[26] J.M. Tarragó, S. Dorvlo, J. Esteve, L. Llanes, Influence of the microstructure on the thermal shock behavior of cemented carbides, Ceram. Int. 42 (2016) 12701–12708. doi:10.1016/j.ceramint.2016.05.024.

[27] M.D. Uchic, P.A. Shade, D.M. Dimiduk, Plasticity of micrometer-scale single crystals in compression, Annu. Rev. Mater. Res. 39 (2009) 361–386. doi:10.1146/annurev-matsci-082908-145422.

[28] R. Dou, B. Derby, A universal scaling law for the strength of metal micropillars and nanowires, Scr. Mater. 61 (2009) 524–527. doi:10.1016/j.scriptamat.2009.05.012.

[29] P.S.S. Leung, A.H.W. Ngan, Size effect on the strength of micron-sized polycrystals – A dislocation dynamics simulation study, Scr. Mater. 69 (2013) 235–238. doi:10.1016/j.scriptamat.2013.04.006.

[30] J.J. Roa, E. Jiménez-Piqué, J.M. Tarragó, D.A. Sandoval, A. Mateo, J. Fair, L. Llanes, Hall-Petch strengthening of the constrained metallic binder in WC–Co cemented carbides: Experimental assessment by means of massive nanoindentation and statistical analysis, Mater. Sci. Eng. A. 676 (2016) 487–491. doi:10.1016/j.msea.2016.09.020.

[31] H. Fei, A. Abraham, N. Chawla, H. Jiang, Evaluation of micro-pillar compression tests for accurate determination of elastic-plastic constitutive relations, J. Appl. Mech. 79 (2012) 061011 1-9. doi:10.1115/1.4006767.

[32] D.P. Adams, M.J. Vasile, Accurate focused ion beam sculpting of silicon using a variable pixel dwell time approach, J. Vac. Sci. Technol. B Microelectron. Nanom. Struct. Process. Meas. Phenom. 24 (2006) 836–844. doi:10.1116/1.2184325.

[33] S. Lay, HRTEM investigation of dislocation interactions in WC, Int. J. Refract. Met. Hard Mater. 41 (2013) 416–421. doi:10.1016/j.ijrmhm.2013.05.017.

[34] L.S. Sigl, H.F. Fischmeister, On the fracture toughness of cemented carbides, Acta Metall. 36 (1988) 887–897. doi:10.1016/0001-6160(88)90143-5.

[35] H.F. Fischmeister, S. Schmauder, L.S. Sigl, Finite element modelling of crack propagation in WC-Co hard metals, Mater. Sci. Eng. A. 105/106 (1988) 305–311.

[36] G.E. Lloyd, Atomic number and crystallographic contrast images with SEM: a review of backscattered electron techniques, Mineral. Mag. 51 (1987) 3–19.

[37] J.J. Roa, E. Jiménez-Piqué, J.M. Tarragó, M. Zivcec, C. Broeckmann, L. Llanes, Berkovich nanoindentation and deformation mechanisms in a hardmetal binder-like cobalt alloy, Mater. Sci. Eng. A. 621 (2015) 128–132. doi:10.1016/j.msea.2014.10.064.

[38] V.K. Sarin, T. Johannesson, On the Deformation of WC-Co Cemented Carbides, Met. Sci. 9 (1975) 472–476.

[39] B. Roebuck, E.A. Almond, A.M. Cottenden, The influence of composition, phase transformation and varying the relative F.C.C. and H.C.P. phase contents on the properties of dilute Co□W□C alloys, Mater. Sci. Eng. 66 (1984) 179–194. doi:10.1016/0025-5416(84)90179-4.

[40] C.H. Vasel, A.D. Krawitz, E.F. Drake, E.A. Kenik, Binder deformation in WC-(Co, Ni) cemented carbide composites, Metall. Trans. A. 16 (1985) 2309–2317. doi:10.1007/BF02670431.

[41] G. Erling, S. Kursawe, S. Luyckx, H.G. Sockel, Stable and unstable fracture surface features in WC-Co, J. Mater. Sci. Lett. 19 (2000) 437–438.

[42] H. Doi, Y. Fujiwara, K. Miyake, Y. Oosawa, A systematic investigation of elastic moduli of Wc-Co alloys, Metall. Mater. Trans. 1 (1970) 1417–1425. doi:10.1007/BF02900264.

List of Tables

List of Figures

Table I: Characteristic dimensions of micropillars obtained, following the described milling procedure.

Diameter denomination in this study (µm)	Micropllar diameter, d_{pillar} (µm)	Aspect ratio, l_{pillar}/d_{pillar}	Taper angle, α (°)
1	1.1 ± 0.4	3.7 ± 1.4	2.5 ± 0.1
2	1.9 ± 0.0	3.7 ± 0.2	2.0 ± 0.1
4	3.8 ± 0.0	2.5 ± 0.0	1.8 ± 0.2

Table II: Maximum test conditions of strain and nanoindentation load imposed for each micropillar size.

Micropillar diameter (μm)	Maximum strain (%)	Maximum indentation load (mN)
1	3.2	15
2	4.0	20
4	8.5	50

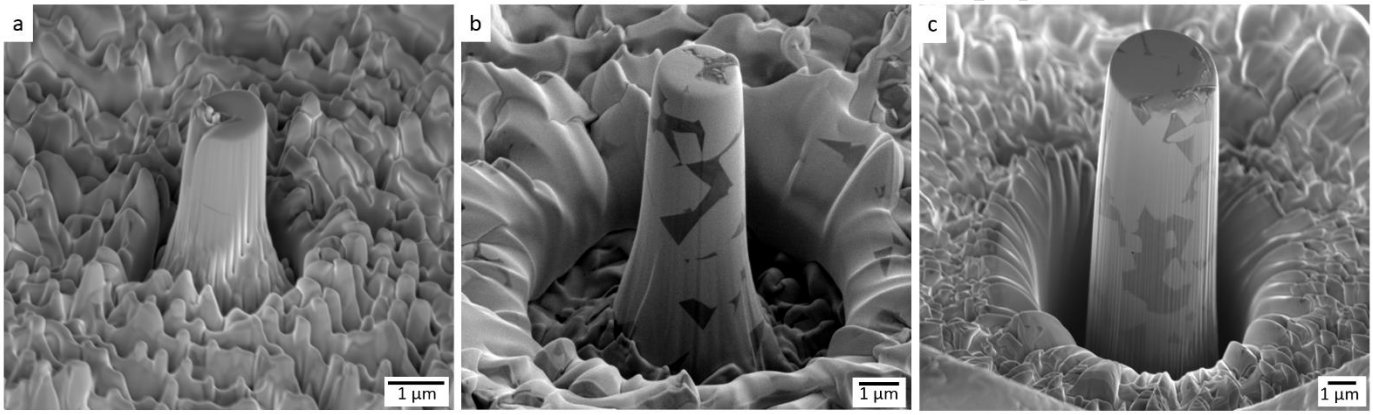

Figure 1: Milled micropillars of (a) 1 µm, (b) 2 µm and (c) 4 µm in diameter.

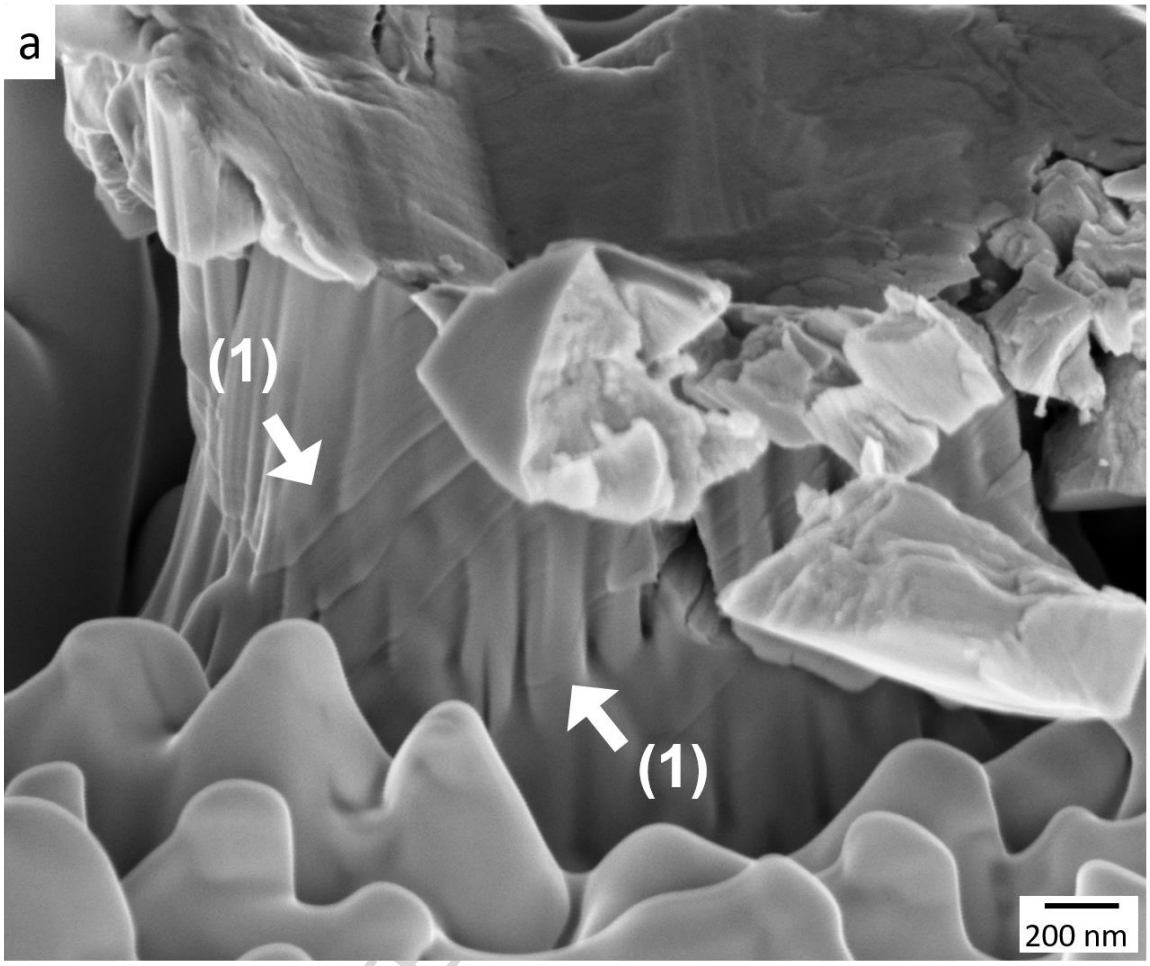

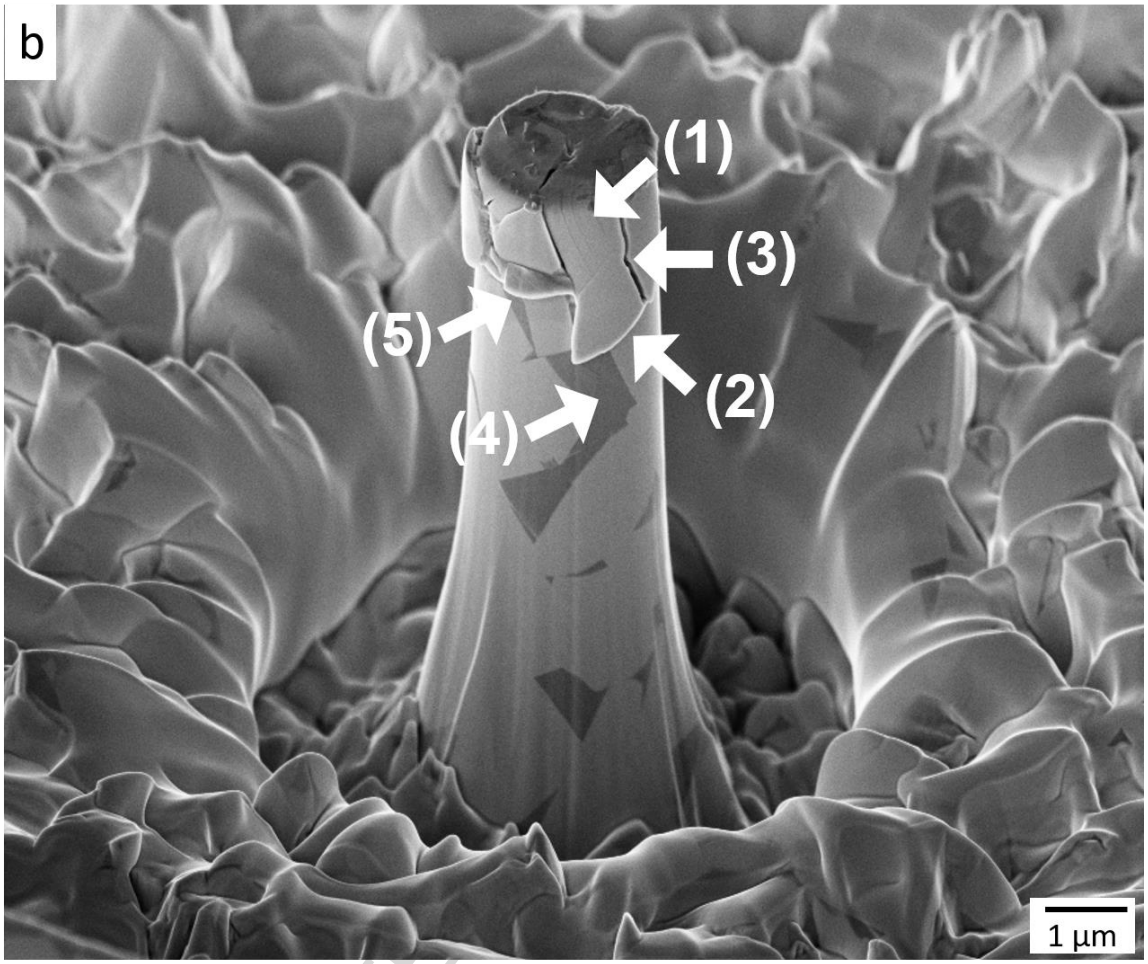

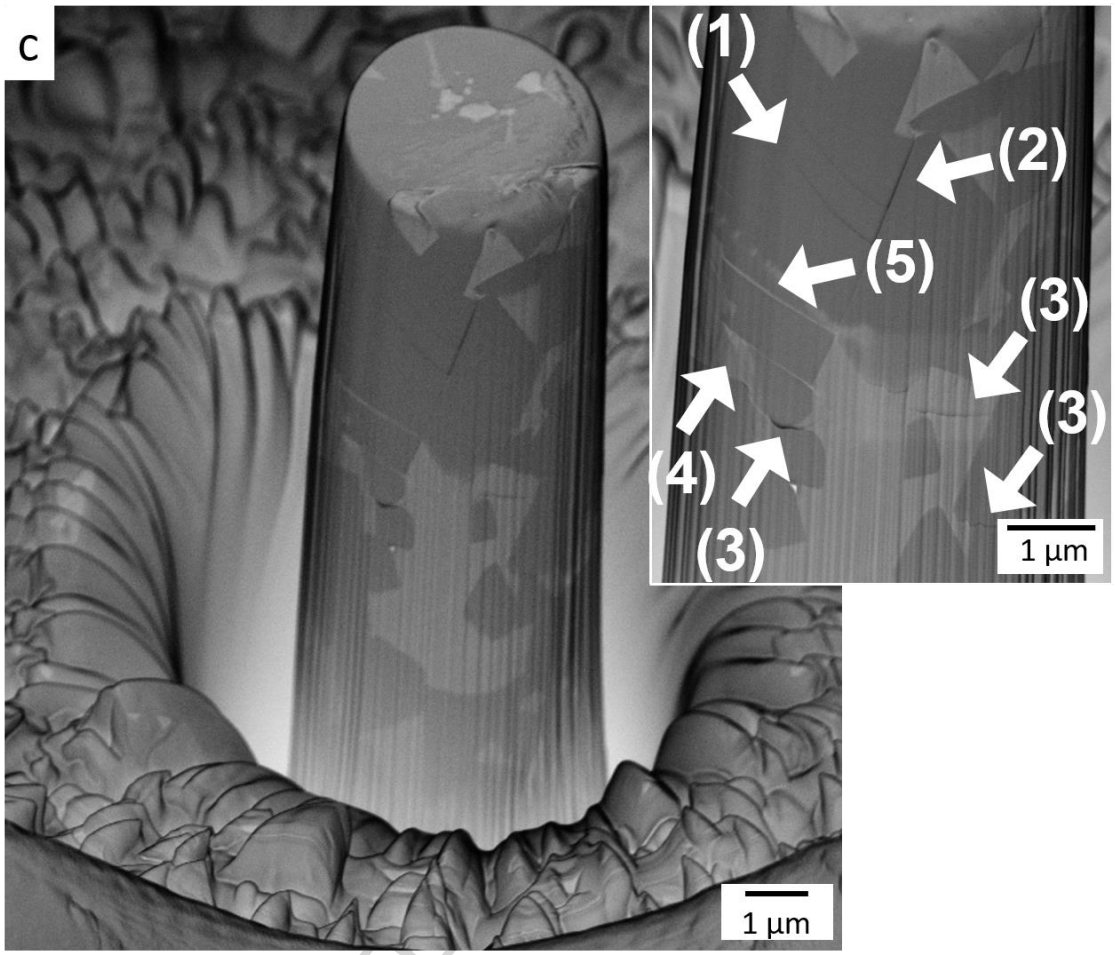

Figure 2: FESEM micrographs evidencing deformation/failure mechanisms after uniaxial compression of the micropillars of a) 1 µm, b) 2 µm, and c) 4 µm. The arrows stands for the mechanisms observed: (1) slip lines in WC particles; (2) glide at the WC/WC interfaces; (3) submicron crack arise in WC/WC and propagation in WC/Co interfaces and Co; (4) plastic deformation within the binder; and (5) flow of the Co binder trough the boundaries of WC particles glided.

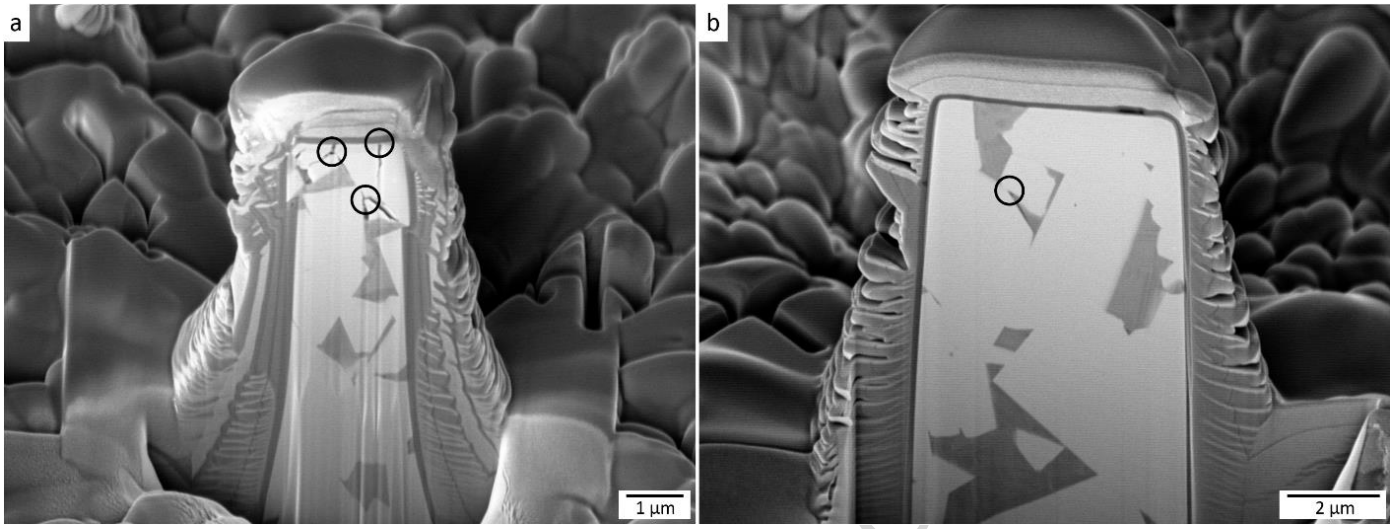

Figure 3: FESEM/FIB images for sectioned micropillars of a) 2 µm and b) 4 µm. The images correspond to near the center of the micropillars. Points of maximum triaxiality are denoted with a black circle.

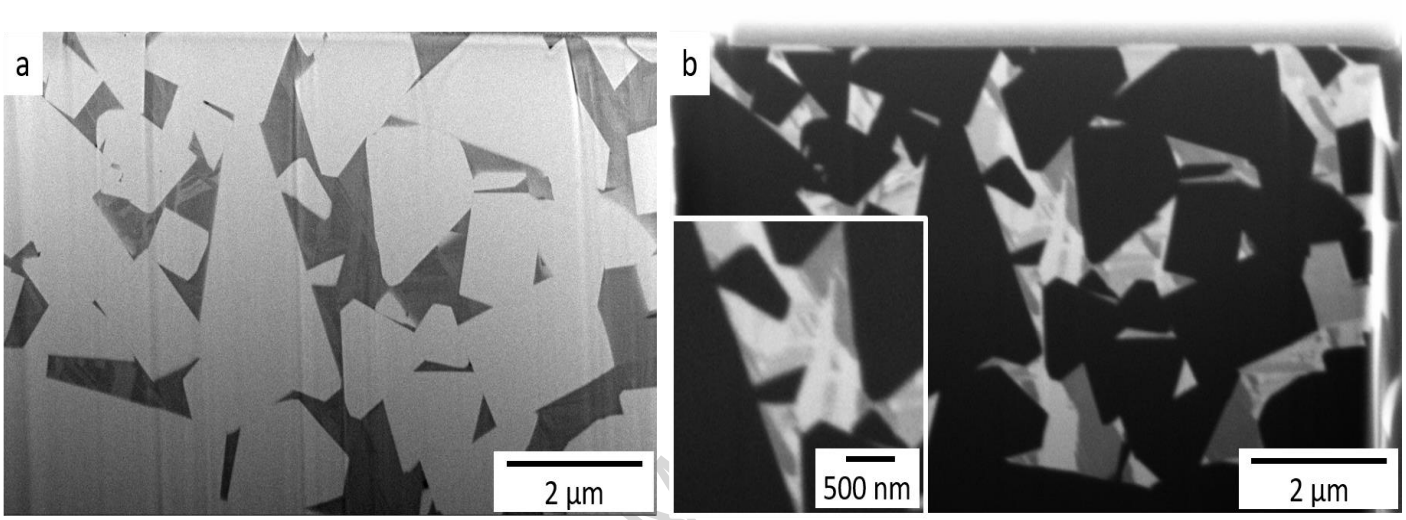

Figure 4: a) SEM and b) FIB images showing a transversal cut of the bulk WC-Co hardmetal by means of FIB. The images were taken with an acceleration voltage of 30 kV and at angle of 36 degrees. Co binder phase corresponds to the darker phase in SEM image and to the lighter phase in FIB image. Magnification of a metallic binder region is found at the left corner of the FIB image. Contrast bands observed within the Co binder correspond to substructural feature associated with crystallographic differences.

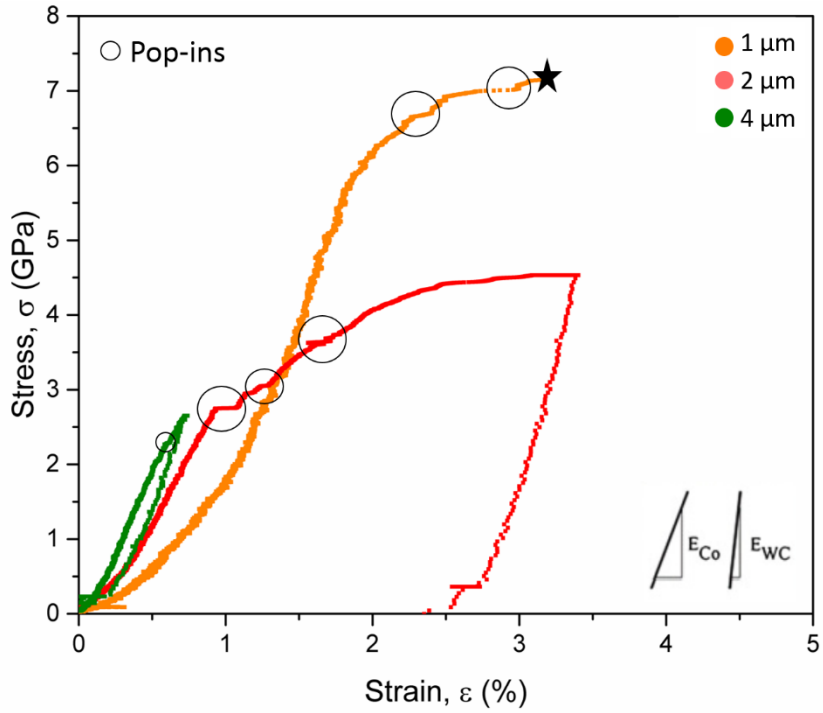

Figure 5: Stress-strain curves drawn from the load-displacement data obtained by uniaxial compression testing of micropillars of 1, 2 and 4 µm in diameter milled on WC-Co cemented carbide. E_{Co} and E_{WC} correspond to elastic modulus for the Co and WC, respectively.

Highlights

- A protocol for evaluation of mechanical behavior of WC-Co at microscale is proposed
- The volume of the sample influences the micromechanical response of WC-Co
- For small volumes the micromechanical response is similar to that of the WC
- Micromechanical response for higher volumes approach to that of the bulk
- Interfaces are preferential sites for emergence of deformation/failure phenomena